International Journal of Heat and Mass Transfer, 131, (2019), 920-931.
doi:10.1016/j.ijheatmasstransfer.2018.11.108

Elucidation of the weld pool convection and keyhole formation mechanism in the keyhole plasma arc welding

Dongsheng Wu*, Anh Van Nguyen**, Shinichi Tashiro***, Xueming Hua****, Manabu Tanaka*****

Abstract (180Words)

An electrode-arc model, and a three dimensional weld pool model considering the self-adaptive heat source, the shear stress caused by plasma flow, and the deformation of the top and bottom surfaces, are developed to investigate the weld pool convection and keyhole formation mechanism in the keyhole plasma arc welding. With the help of the X-ray transmission system, high-speed video camera and thermal camera, the fluid flow and the temperature distribution of the weld pool are studied. The numerical and experimental results show that: after the penetrated keyhole formation, two convective eddies are formed inside the weld pool. The molten metal flows backward at the top surface of the weld pool, and flows downward and backward at the bottom surface of the weld pool. The low temperature distribution in the weld pool is attributed to the strong fluid flow and energy transportation caused by the much high arc pressure and plasma shear stress. Both the arc pressure driven weld pool deformation and shear stress driven weld pool deformation are responsible for the keyhole formation, and the first mechanism is especially dominant.

Keywords

Keyhole plasma arc welding; Self-adaptive heat source; Plasma shear stress; X-ray transmission system

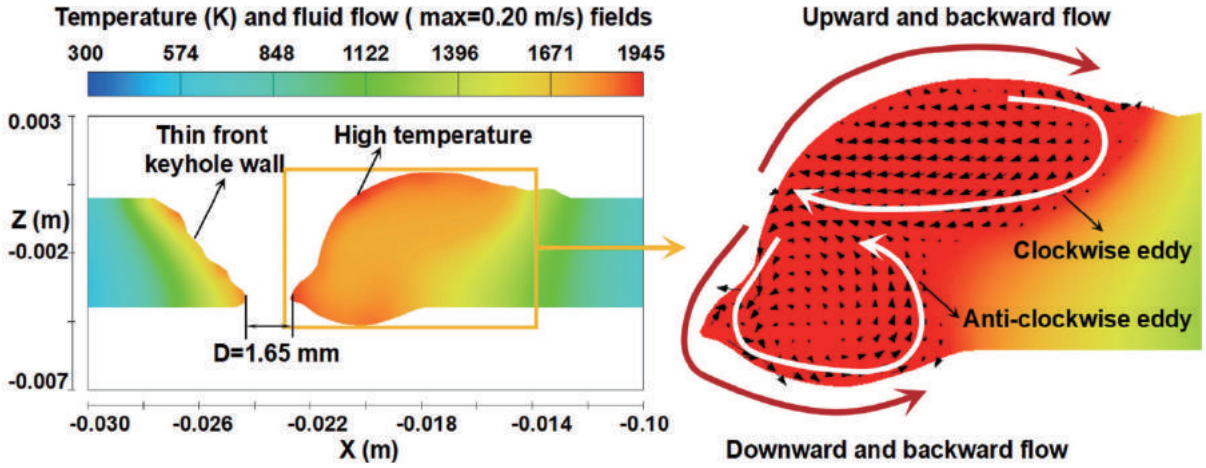

(a) temperature (b) fluid flow fields

Fig.1.
Temperature (K) and fluid flow fields of cross sectional view.

* Graduate School Student
** Murata Welding Laboratories, Ltd
*** Assistant Professor
**** Shanghai Jiao Tong University
***** Professor

Applied Physics Letters, 112, (2018), 152103.
doi:10.1063/1.5011268

Fabrication of high-performance InGaZnOx thin film transistors based on control of oxidation using a low-temperature plasma

Kosuke Takenaka*, Masashi Endo**, Giichiro Uchida*** and Yuichi Setsuhara****

Abstract (146 Words)

This work demonstrated the low-temperature control of the oxidation of a-IGZO films using inductively-coupled plasma as a means of precisely tuning the properties of thin film transistors (TFTs) and as an alternative to post-deposition annealing at high temperatures. The effects of the plasma treatment of as-deposited a-IGZO films were investigated by assessing the electrical properties of TFTs incorporating these films. A TFT fabricated using an a-IGZO film exposed to an Ar-H_2-O_2 plasma at substrate temperatures as low as 300 °C exhibited the best performance, with a field effect mobility as high as 42.2 $cm^2V^{-1}s^{-1}$, a subthreshold gate voltage swing of 1.2 V $decade^{-1}$ and a threshold voltage of 2.8 V. The improved transfer characteristics of TFTs fabricated with a-IGZO thin films treated using an Ar-H_2-O_2 plasma are attributed to the termination of oxygen vacancies around Ga and Zn atoms by OH radicals in the gas phase.

Keywords

InGaZnOx; Thin film transistor; Post deposition process; Plasma assisted reactive sputtering

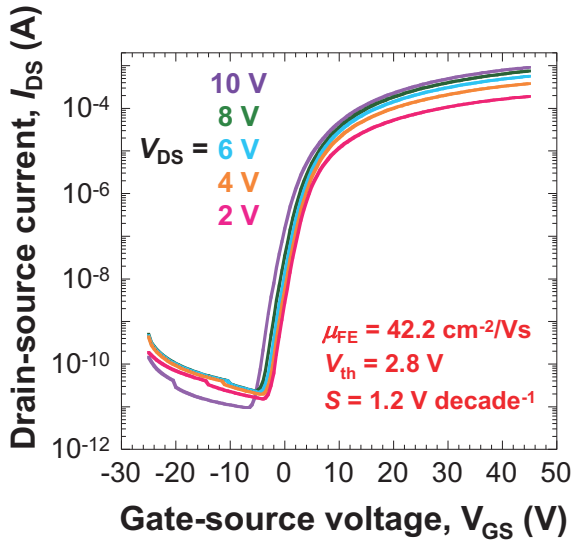

Fig.1
Transfer characteristics of IGZO TFTs fabricated using (a) as-deposited a-IGZO film and a-IGZO films treated with Ar-H_2-O_2 plasmas. Reproduced from Applied Physics Letters, 112 (2018) 152103, with the permission of AIP Publishing.

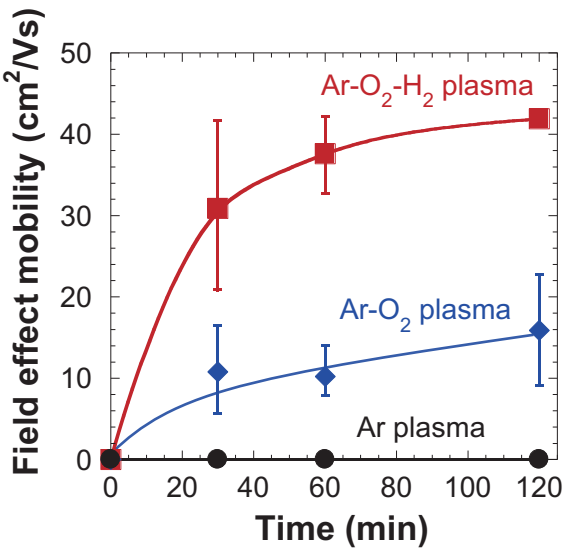

Fig.2
Field effect mobility values (IFE) for IGZO TFTs fabricated using a-IGZO thin films treated with Ar, Ar-O_2, and Ar-H_2-O_2 plasmas. Reproduced from Applied Physics Letters, 112 (2018) 152103, with the permission of AIP Publishing.

* Assistant Professor
** Graduate School Student
*** Associate Professor
**** Professor

Journal of alloy and compounds, 765, (2018), 1243-1252.
doi:10.1016/j.jallcom.2018.06.121

Improvement in the mechanical properties of eutectic Sn58Bi alloy by 0.5 and 1 wt% Zn addition before and after thermal aging

Shiqi Zhou*, Omid Mokhtari**, Muhammad Ghufran Rafique***, Vasanth C. Shunmugasamy***, Bilal Mansoor***, Hiroshi Nishikawa**

Abstract (138 Words)

A comparative analysis of the microstructure and the mechanical properties of the eutectic Sn58Bi, 0.5 wt% and 1 wt% zinc (Zn)-functionalized Sn58Bi alloys was conducted before and after solid-state thermal aging. In addition, the mechanical properties of individual Sn and Bi phases were obtained using nanoindentation tests. The results indicated that finer microstructures were obtained in the Zn-added samples compared to the eutectic Sn58Bi before and after aging since the Sn–Bi phase boundary segregation of Zn occurred during aging, and the movement of the diffusion entities (Sn and Bi atoms) through the boundaries was obstructed. The fine microstructure was responsible for the ultimate tensile strength improvement obtained in the Zn-added samples. Meanwhile, a significant hardness decrease of the Sn phase in the Sn58Bi1Zn alloy was believed to be a possible reason for the superior elongation of the Zn-added samples.

Keywords

Sn-Bi alloys, Tensile test, Nanoindentation, Phase boundary, Solid solute softening

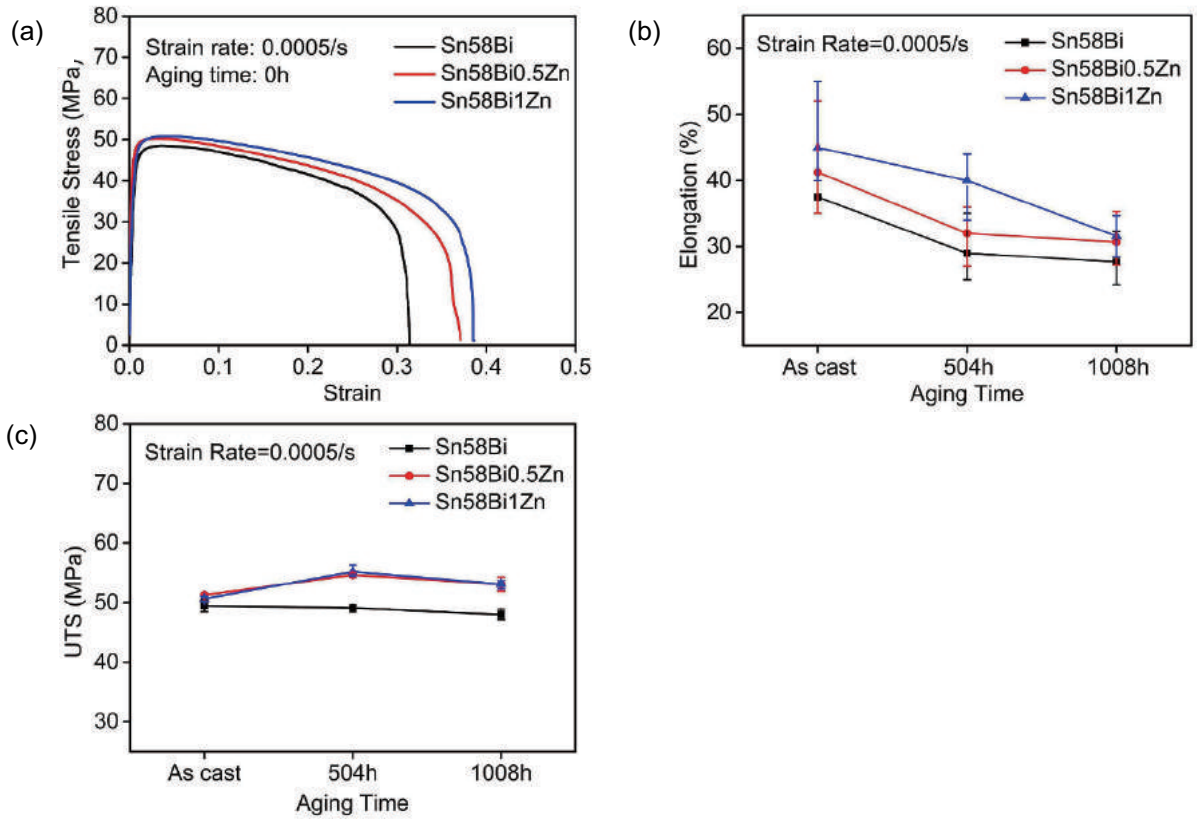

Fig. 1 (a) Tensile stain-stress curves of eutectic Sn58Bi and Zn added Sn58Bi solder slabs before aging. (b) Elongations of eutectic Sn58Bi and Zn added Sn58Bi before and after aging. (c) UTSs of eutectic Sn58Bi and Zn added Sn58Bi before and after aging.

* Graduate School Student
** Associate Professor
*** Texas A&M University at Qatar

Sato, Y., Tsukamoto, M., Shobu, T. et al. Appl. Phys. A, (2018) 124: 288
doi:10.1007/s00339-018-1712-4

Preheat effect on titanium plate fabricated by sputter-free selective laser melting in vacuum

Yuji Sato*, Masahiro Tsukamoto**, Takahisa Shobu***, Yorihiro Yamashita****, Shuto Yamagata*****, Takaya Nishi*****, Ritsuko Higashino*******, Tomomasa Ohkubo*******, Hitoshi Nakano********, Nobuyuki Abe*********

Abstract (120 Words)

The dynamics of titanium (Ti) melted by laser irradiation was investigated in a synchrotron radiation experiment. As an indicator of wettability, the contact angle between a selective laser melting (SLM) baseplate (SUS304 stainless steel) and the molten Ti (particle size: 200 μm) was measured by synchrotron X-rays at 30 keV during laser irradiation. As the baseplate temperature increased, the contact angle decreased, down to 28° at a baseplate temperature of 500°C. Fig.1 shows Contact angle between molten Ti particle and baseplate at 500°C. Based on this result, the influence of wettability of a Ti plate fabricated by SLM in a vacuum was investigated. It was revealed that the improvement of wettability by preheating suppressed sputtering generation, and a surface having a small surface roughness was fabricated by SLM in a vacuum.

Keywords

selective laser melting（SLM）; sputter-free; synchrotron X-rays; vacuum

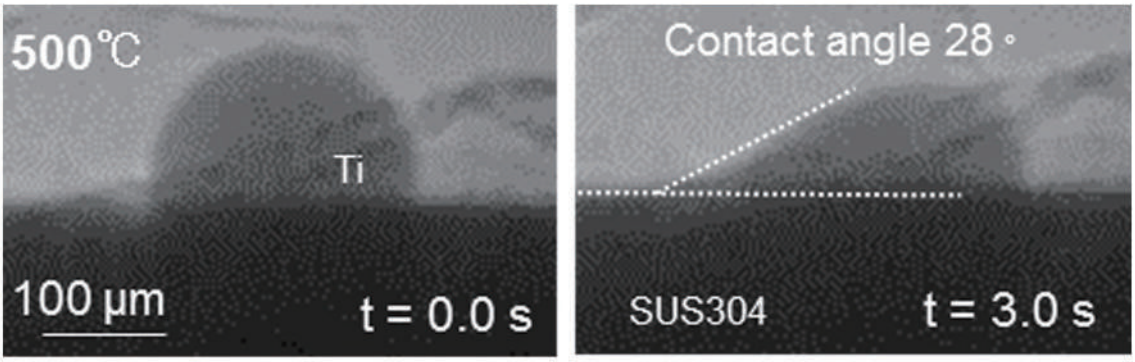

Fig1.. Contact angle between molten Ti particle and baseplate at 500°C.

* Specially Appointed Associate Professor
** Professor
*** Japan Atomic Energy Agency
**** Industrial Research Institute of Ishikawa
***** Graduate School Student
****** Specially Appointed Researcher
******* Tokyo University of Technology
******** Kindai University
********* Specially Appointed Professor

Materials & Design, 160, (2018), 1019–1028.
doi:10.1016/j.matdes.2018.10.036

Weld Toe Modification Using Spherical-tip WC Tool FSP in Fatigue Strength Improvement of High-strength Low-alloy Steel Joints

Hajime Yamamoto*, Yoshikazu Danno*, Kazuhiro Ito**, Yoshiki Mikami***, Hidetoshi Fujii**

Abstract (191Words)

Fatigue strength of fusion-welded joints is lower than that of the base metal due to stress concentration, tensile residual stress, and microstructural degradation at the weld toe. To improve these issues, friction stir processing (FSP) using a spherical tip tool was directly applied to the weld toe of high-strength low-alloy steel joints. The toe geometry was successfully modified without defect formation, resulting in 25% reduction in fatigue notch factor in comparison to the as-welded joints. Significant grain refinement due to FSP increased hardness beneath the toe surface. In addition, compressive residual stress related to tool wear was produced on the FSP surface. Bending fatigue strength was improved by these benefits, with dependence on the tool travel speed. Fatigue crack initiation occurred at the toe surface for all the joints. Although high travel speed FSP produced serrated surface resulting in degradation of FSP improvement in fatigue strength, low travel speed FSP contributed to reduction of surface roughness leading to maximum FSP improvement of 50% in fatigue strength. The results obtained in this study suggest the encouraging prospect of direct application of FSP to weld toes as new post-weld treatment for steel joints.

Keywords

Friction stir processing; Post-weld treatment; High-strength low-alloy steel; Fatigue strength; Weld geometry; Residual stress

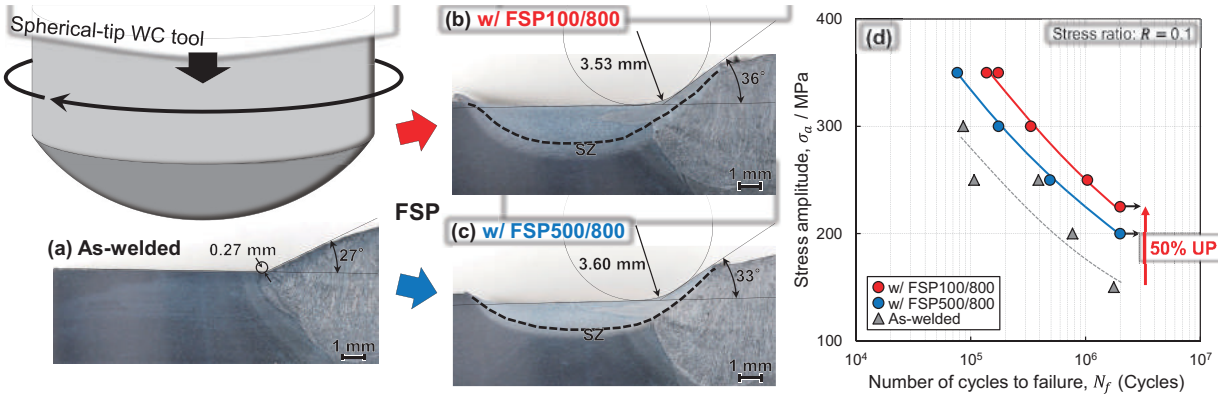

Fig. 1. Cross-sectional OM images of joint (a) as-welded and with (b) FSP100/800 and (c) FSP500/800 (the tool travel speed of 100 and 500 mm/min, respectively, at the constant tool rotational speed of 800 rpm), and (d) their S-N curves obtained by four-point bending fatigue tests, together with that of the base metal.

* Graduate School Student
** Professor
*** Associate Professor

Research Division of Materials Joining Mechanism, Dep. of Joint Interface Structure and Formation Mechanism

Acta Materialia, 148, (2018), 235–248.
doi:10.1016/j.actamat.2018.02.004

Stacking-fault energy, mechanical twinning and strain hardening of Fe-18Mn-0.6C-(0, 1.5)Al twinning-induced plasticity steels during friction stir welding

Seung-Joon Lee*, Yufeng Sun**, Hidetoshi Fujii***

Abstract (179 Words)

The effect of friction stir welding (FSW) on the microstructure, stacking-fault energy (SFE) and strain hardening rate (SHR) of Fe-18Mn-0.6C-(0 and 1.5)Al (wt.%) twinning-induced plasticity steels using three welding speeds (50, 100 and 200 mm min^{-1}) was investigated. The yield strength of the FSWed 0Al and 1.5Al steels improved due to both the grain refinement and introduced dislocations with increasing welding speed. The SHR with three stages and without the yield drop increased due to active twinning and accumulated dislocations during FSW with higher welding speed. The 0Al-200 steel with a fine grain exhibited more active twinning than the coarse-grained specimen (0Al-50), contrast to the 1.5Al steel. Regardless of the specimens, the slight increase in the SFE, which was attributed to both the shear strain energy and the excess free energy during FSW, leads to an increase in the critical twinning stress (σ_{tw}). Despite the fine grain of 0Al steel, the origin of its active twinning was the highly increased yield strength relative to σ_{tw}, and the promoted dislocation interactions, leading to an increase in the number of twin nucleation sites.

Keywords

Friction stir welding (FSW); Deformation twinning; Stacking-fault energy (SFE); Thermodynamic modeling; Twinning-induced plasticity (TWIP) steel

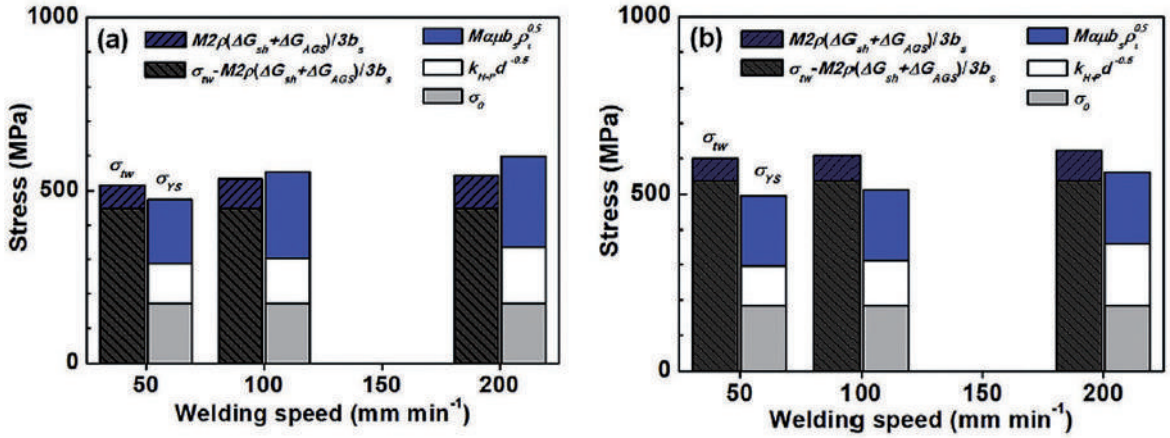

Fig. 1. Variations in calculated critical stress for mechanical twinning (σ_{tw}) along with the experimental yield strength (YS) of (a) 0Al and (b) 1.5Al steels with an increase in the welding speed from 50 to 200 mm min^{-1}.

* Specially appointed assistant professor
** Specially appointed associate professor
*** Professor

Materials Science & Engineering A, 739, (2019), 491-498.
doi: 10.1016/J.MSEA.2018.10.081

Microstructural and mechanical properties of α-titanium sintered material via thermal decomposition of additive chromium oxide particles

Kondoh Katsuyoshi*, Ikemasu Ryuho**, Umeda Junko***, Kariya Shota**, Anak Khantachawana****

Abstract (145 Words)

The pre-mixed pure Ti and Cr_2O_3 powder was consolidated by spark plasma sintering (SPS) and hot extrusion to fabricate α-titanium (Ti) materials with oxygen (O) and chromium (Cr) elements by powder metallurgy (PM) process. The Cr_2O_3 particles were completely decomposed during SPS, and then O and Cr atoms were dissolved in α-Ti matrix. Oxygen atoms were remarkably improved the mechanical strength of PM Ti-O-Cr alloys by their solid solution hardening effect. The Cr solution and Ti_4Cr precipitates had important roles to obstruct the grains coarsening behavior by the solute drag and Zener pinning effects, respectively. The solid solution strengthening effect by Cr atoms, however, was very limited due to a small Cr solubility of about 0.35 at% in α-Ti phase of Ti-OCr alloys. Since Ti4Cr precipitates with 10‐20 μm diameters were not so fine, they hardly contributed to the precipitation hardening of Ti-O-Cr alloys.

Keywords

Powder metallurgy; Titanium; Chromium oxide; Solid solution; Grain refinement; Zener pinning; Solute drag

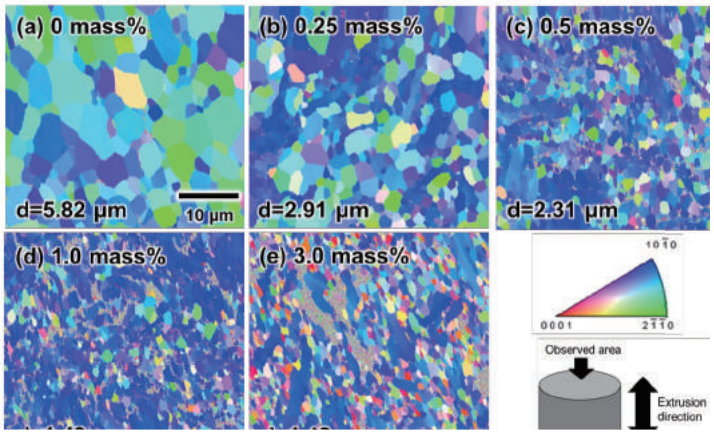

Fig. 1 Inverse pole figure (IPF) maps of extruded Ti-Cr_2O_3 materials and mean grain size, where Cr_2O_3 contents is 0 mass% (a), 0.25 mass% (b), 0.5 mass% (c), 1.0 mass%(d) and 3.0 mass% (e).

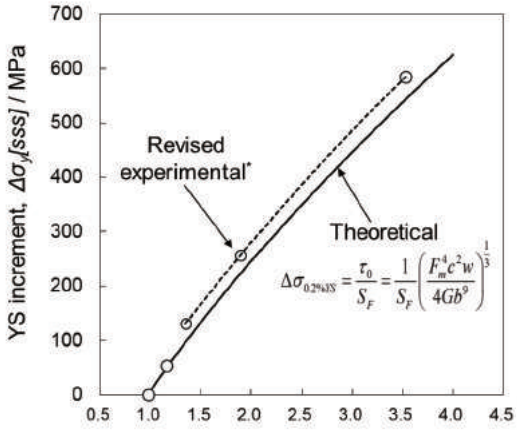

Fig. 2 YS increment of theoretical using Labusch model and revised experimental* as function of oxygen content of extruded Ti-Cr_2O_3 materials. *Effect of grain refinement on YS increment was removed from original experimental values.

* Professor
** Graduate Student
*** Associate Professor
**** King Mongkut's University of Technology Thonburi, Thailand

Materials and Design, 155, (2018), 384–395.
doi:10.1016/j.matdes.2018.06.024

Deposition behavior, microstructure and mechanical properties of an in-situ micro-forging assisted cold spray enabled additively manufactured Inconel 718 alloy

Xiao-Tao Luo*, Meng-Lin Yao*, Ninshu Ma**, Makoto Takahashi***, Chang-Jiu Li*

Abstract (202 Words)

Cold spray is capable to additively manufacture oxide-free metallic parts in open air due to its low processing temperature. However, for metals with relatively high hardness such as Inconel 718 super alloy (IN718), it is still a big challenge to get dense deposits by using low-priced nitrogen gas. In this work, In-situ micro-forging (MF) was introduced to cold spray by mechanically mixing big-sized 410 stainless steel (410SS) particles into the IN718 powder so that the deposited IN718 layer can be hammered and plastically deformed by the MF particles during spraying and results in fully dense deposits. As 50 vol%MF particles were mixed into the IN718 powder, the porosity was decreased from 5.6% to 0.26%. Due to the low impact velocity, 410SS particles were not embedded into the IN718 deposits and the possible contamination was avoided. An oxide scale removal induced increment in deposition efficiency was detected for the first time. Due to the lower porosity and enhanced interparticle bonding, a great improvement in ultimate strength from 96 to 464 MPa was achieved by the in-situ MF effect. After heat treated at 1200 °C for 6 h, the sample fractured at a high strength of 1089 MPa and revealed a ductile fracture manner.

Keywords

Additive manufacturing; Cold spray; In-situ micro-forging; Microstructure; Mechanical properties

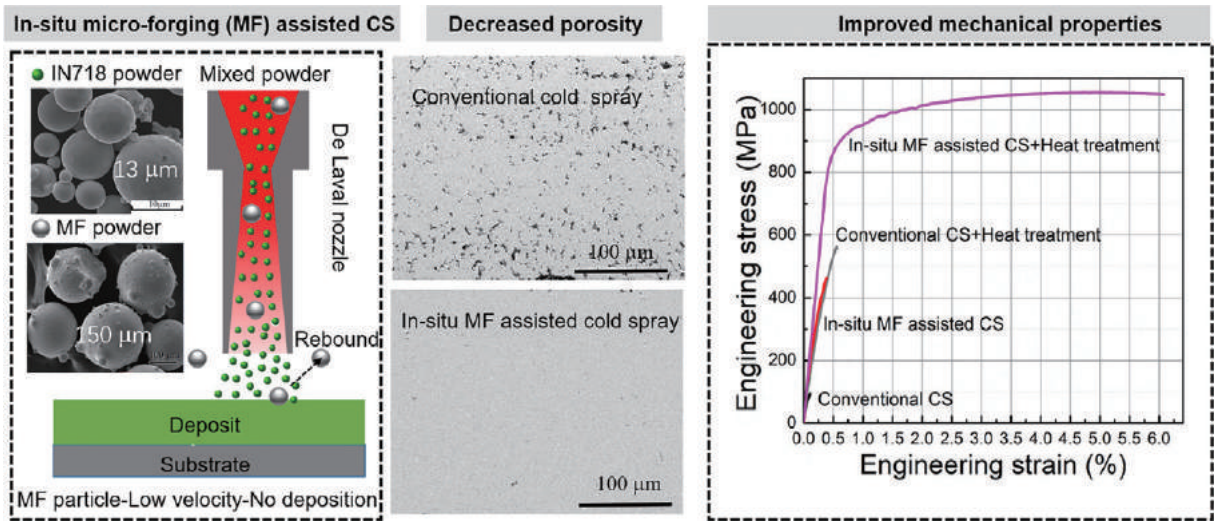

Fig.1.Schematic representation of in-situ micro-forging assisted cold-spray process for additive manufacture, microstructure and mechanical properties

* Xian Jiaotong University
** Professor
*** Associate Professor

Engineering Fracture Mechanics, 187, (2018), 142–164.
doi:10.1016/j.engfracmech.2017.10.034

Fracture Assessment Procedure Developed in Japan for Steel Structures under Seismic Conditions

Fumiyoshi Minami*, Yasuhito Takashima**, Mitsuru Ohata***, Yusuke Shimada****, Takahiko Suzuki*****, Hiroshi Shimanuki******, Satoshi Igi*******, Takumi Ishii********, Masao Kinefuchi*********, Tetsuo Yamaguchi**********, Yukito Hagihara**********

Abstract (145Words)

The Engineering Standard, WES 2808, has been developed in Japan for assessing the brittle fracture of steel-framed components at the earthquake. This paper describes the key contents of WES 2808 and demonstrates the application to beam-to-column connections. WES 2808 includes two unique ideas: (1) a reference temperature concept for the evaluation of the material fracture toughness under cyclic and dynamic loading, and (2) an equivalent CTOD concept for the correction of CTOD toughness for constraint loss in structural components. A skeleton strain is employed to define the pre-strain prior to fracture during cyclic loading. The revision of WES 2808 has been done in 2017 to expand the range of use and to improve the accuracy of CTOD toughness correction on the basis of ISO 27306-2016. It is shown that fracture strains of beam-to-column subassemblies predicted by WES 2808 are in a good agreement with those measured.

Keywords

Brittle fracture; Steel structures; Cyclic loading; Dynamic loading; Pre-strain

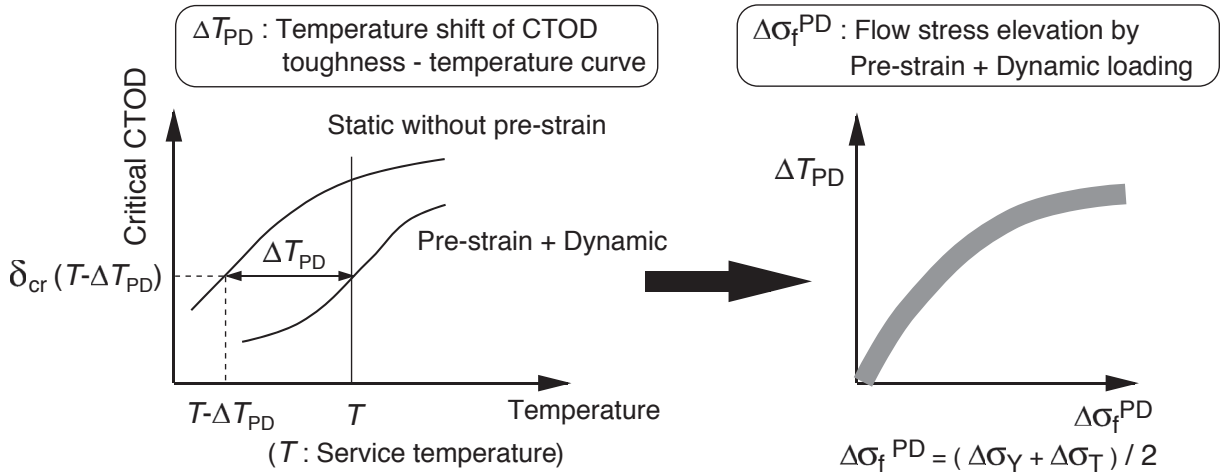

Fig. 1.
Reference temperature concept for evaluation of material fracture toughness under seismic conditions.

*	Professor	*******	JFE Steel Corporation
**	Assistant Professor	********	JFE Techno-Research Corporation
***	Osaka University	*********	Kobe Steel
****	Nippon Steel & Sumitomo Metal Corporation	**********	Kobe Steel
*****	Nippon Steel & Sumikin Technology	**********	Sophia University
******	Nippon Steel & Sumitomo Metal Corporation		

Materials & Design, 165, (2019), 107573.
doi:10.1016/j.matdes.2018.107573

Cyclic plasticity model for fatigue with softening behaviour below macroscopic yielding

Seiichiro Tsutsumi*, Riccardo Fincato**

Abstract (115Words)

Experimental observations have evidenced the insufficiency of yield surface definition via monotonic loading to guarantee adequate description of material behaviour under fatigue tests. Therefore, mechanical property characterisation through simple experimental tests such as uniaxial monotonic extension/compression is favoured, considering different responses due to cyclic loading. Herein, a cyclic plasticity model is formulated to capture the correct generation of plastic deformation under cyclic loading conditions, even for stress states lower than the yield stress. Implicit integration strategies, in the form of the cutting-plane and closest projection point return mapping algorithms, are implemented to reduce the computation time. The solution accuracies are compared to that of a forward Euler integration scheme, and exhibit fast and accurate performance.

Keywords

Fatigue; Cyclic plasticity; Cyclic softening behavior; Macroscopic yielding; Crack initiation.

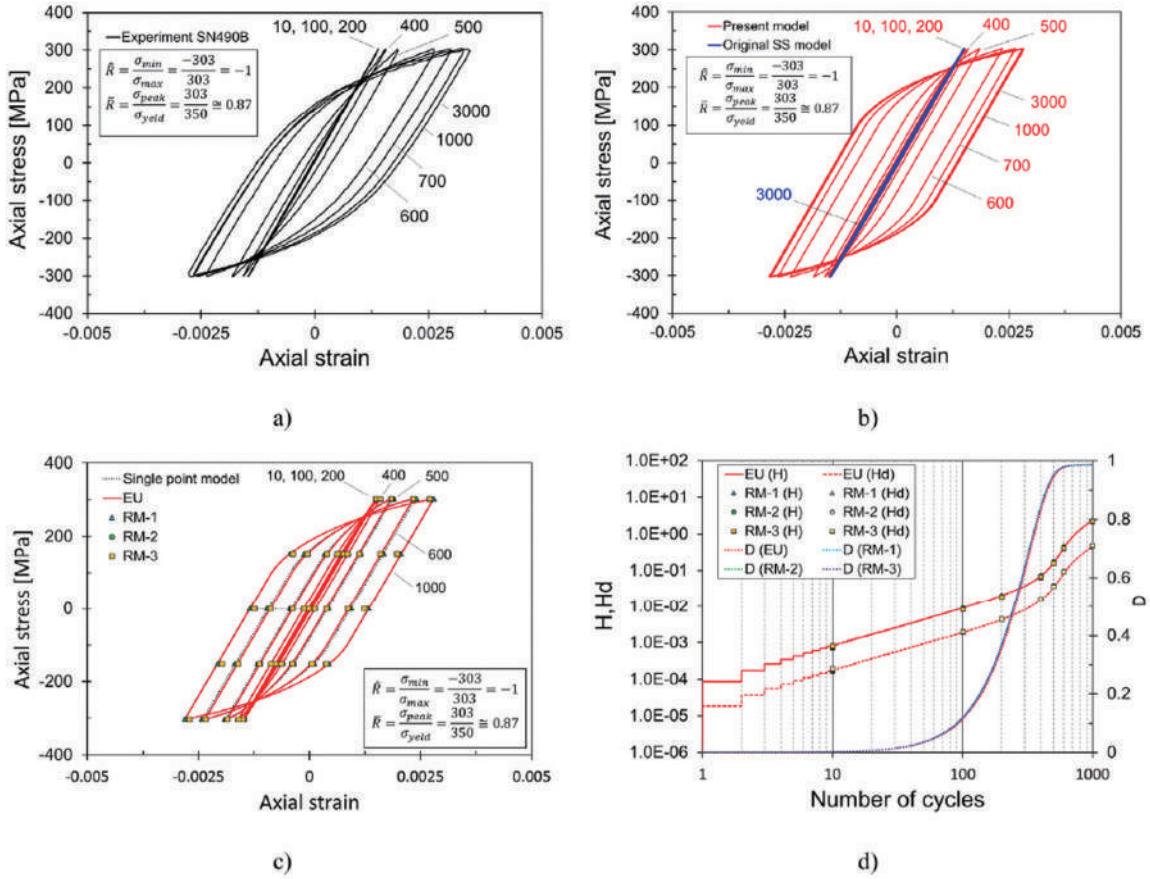

Fig.
Axial stress vs. axial strain for σ_{max}= 303MPa: a) experiment, b) model response EU, c) comparison among the single point model, the forward Euler scheme (EU), the return mapping (CPM). d) Cumulative plastic strain variables and damage evolution for CPM vs. EU.

* Associate Professor
** Specially Appointed Assistant Professor

Research Division of Materials Joining Assessment, Dep. of Reliability Evaluation &Simulation

Solid State Phenomena, 285, (2019), 277–282.
doi:10.4028/www.scientific.net/SSP.285.277

Analysis of the 355 Aluminium Alloy Microstructure for Application in Thixoforming

Leandro Cássio de Paula*, Shun Tokita**, Kota Kadoi***, Hiroshige Inoue****
and Eugênio José Zoqui*

Abstract (149Words)

The 355 aluminium alloy is known to have excellent thermodynamic characteristics that render it suitable as a raw material for rheocasting and thixoforming. However, besides the controllable transition from solid to liquid phase, the refined microstructure required in the semisolid range is one of the key factors with a strong influence on the rheology of the material. This paper intends to analyze the in situ behavior of the microstructure, in terms of morphological change, using high-temperature laser scanning confocal microscopy. The 355 alloy was prepared via conventional casting, and refined by ultrasonic melt treatment (UST). The specimens were reheated up to the thixoforming temperature and cooled in water. The samples subjected to UST prior to the heat treatment exhibited reduction in grain size, smallest primary phase particle size, and high circularity shape factor. In situ observation methods were employed to analyse evolution mechanisms such as Ostwald ripening and coalescence.

Keywords

Aluminium Alloys, Microstructure, Ultrasonic Melt Treatment, In situ Microstructure Observation

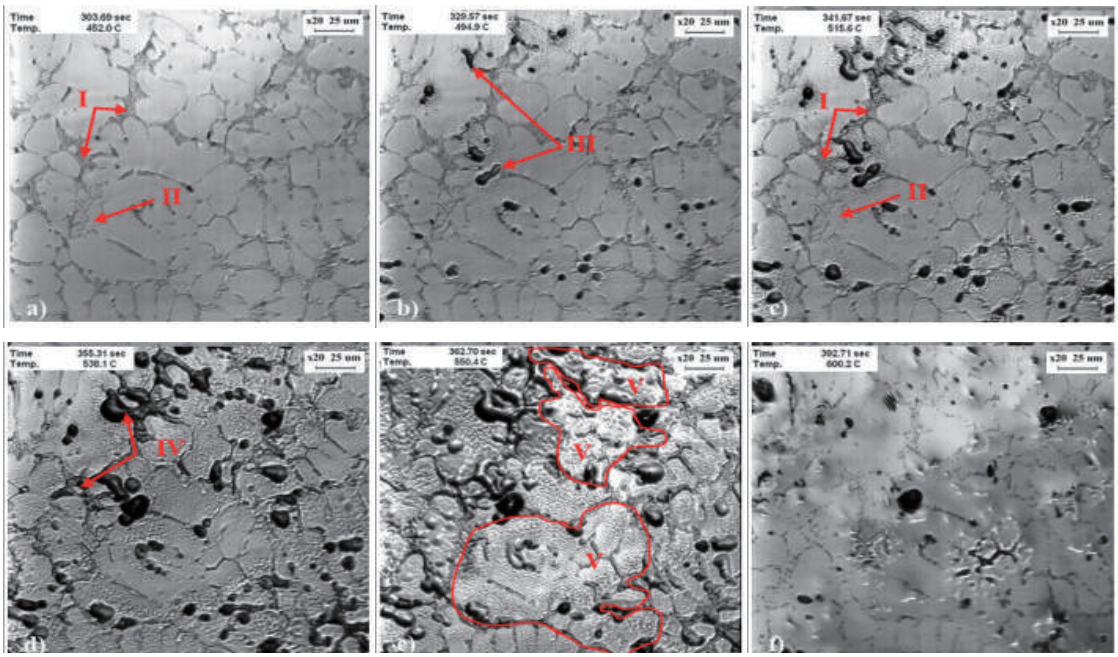

Fig.
Sequence (a-f) of in situ heating obtained by HT-CLSM technique for transformation of 355 aluminium alloy from solid to liquid.

* University of Campinas
** Assistant Professor
*** Associate Professor
**** Professor

Journal of Solid State Chemistry, 263, (2018), 94–99.
doi:10.1016/j.jssc.2018.04.020

Low-temperature synthesis of $LiNi_{0.5}Mn_{1.5}O_4$ grains using a water vapor-assisted solid-state reaction

Takahiro Kozawa*, Daiki Hirobe**, Kunika Uehara***, Makio Naito****

Abstract (194 Words)

$LiNi_{0.5}Mn_{1.5}O_4$ (LNMO) spinel is one of the candidates for the cathodes of high-energy lithium-ion batteries because of its high operating voltage of 4.7 V. However, its use at high voltages leads to the decomposition of common organic electrolytes, resulting in a cycle degradation of the batteries. Although morphological control of LNMO particles involving their size and shape is an effective approach to suppressing electrolyte decomposition, the particle growth relying on diffusion in the solids has limitations of temperature and time. Here, we report the particle growth of LNMO at a low temperature using water vapor. By heating porous Mn_2O_3 spheres with Li and Ni sources as a precursor, we obtain spherical LNMO particles at 500 °C in both air and water vapor. The growth of primary particles is promoted by water vapor, and consequently, the obtained LNMO cathode exhibits better properties than those observed in air. Water vapor also affects the change of shape of LNMO at higher temperatures, leading to the formation of truncated particles from the spheres. Compared to conventional heating processes, this water vapor-assisted particle growth offers a low-temperature control of particle morphologies, particularly for materials that decompose easily at high temperatures.

Keywords

$LiNi_{0.5}Mn_{1.5}O_4$; Lithium-ion batteries; Water vapor; Particle growth; Solid-state reaction

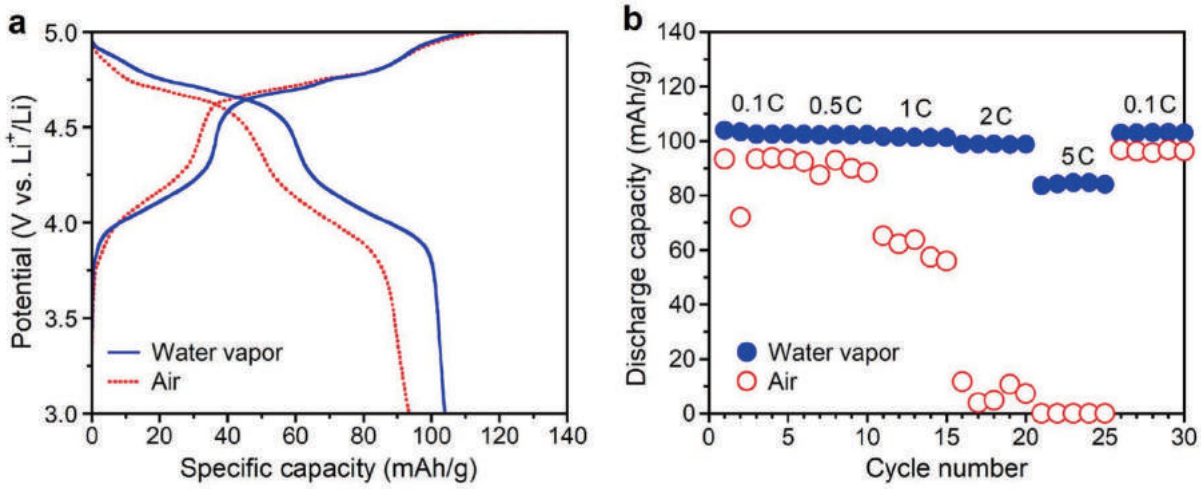

Fig. (a) Charge and discharge curves at the first cycle, measured at the rate of 0.1C, and (b) rate properties of the LNMO cathodes obtained in both the atmospheres at 500 °C.

* Assistant Professor
** Graduate School Student
*** Technical Staff (Technical Expert Division)
**** Professor

Materials, 11, (2018), 835-844
doi:10.3390/ma11050835

Ultraviolet Laser Lithography of Titania Photonic Crystals for Terahertz-Wave Modulation

Soshu Kirihara*, Koki Nonaka**, Shoichiro Kisanuki**, Hirotoshi Nozaki**,
Keito Sakaguchi**

Abstract (186 Words)

Abstract: Three-dimensional (3D) microphotonic crystals with a diamond structure composed of titania microlattices were fabricated using ultraviolet laser lithography, and the bandgap properties in the terahertz (THz) electromagnetic-wave frequency region were investigated. An acrylic resin paste with titania fine particle dispersions was used as the raw material for additive manufacturing. By scanning a spread paste surface with an ultraviolet laser beam, two-dimensional solid patterns were dewaxed and sintered. Subsequently, 3D structures with a relative density of 97% were created via layer lamination and joining as indicated conditions in Table 1. A titania diamond lattice with a lattice constant density of 240 μm was obtained as shown in Fig. 1. The properties of the electromagnetic wave were measured using a THz time-domain spectrometer. In the transmission spectra for the G-X <100> direction, a forbidden band was observed from 0.26 THz to 0.44 THz. The frequency range of the bandgap agreed well with calculated results obtained using the plane–wave expansion method. Additionally, results of a simulation via transmission-line modeling indicated that a localized mode can be obtained by introducing a plane defect between twinned diamond lattice structures.

Keywords

Photonic crystal; Terahertz wave modulation; Additive manufacturing; Ultraviolet laser lithography; Titanium dioxide; Nanoparticles paste

Table 1. Process conditions in ultraviolet laser lithography.

Laser Conditions	A	B	C
Spot Size (μm)	10	10	10
Scan Speed (mm/s	50	100	100
Irradiation Power (mW)	600	600	700

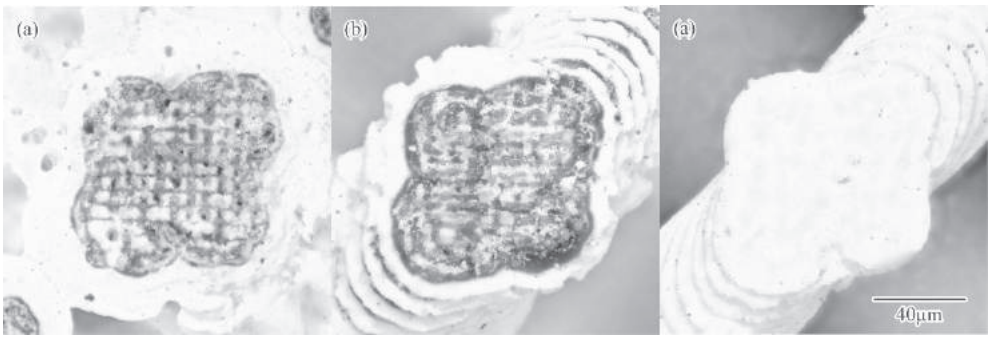

Figure 1. Titania photonic crystals with diamond structures fabricated via ultraviolet laser lithography. The laser-beam irradiation power and the scanning speed were optimized to increase the part accuracy and reduce the amount of remaining carbon. The ceramic lattices (a–c) were fabricated according to the laser conditions A, B and C, indicated in Table 1, respectively.

* Professor
** Graduate Student

Ceramics International, 44, 14 (2018), 17562-17565.
doi:10.1016/j.ceramint.2018.06.170

Facile synthesis of > 99% phase-pure brookite TiO_2 by hydrothermal conversion from Mg_2TiO_4

Mitsuyoshi Machida*, Mariko Kobayashi*, Yoshikazu Suzuki*, Hiroya Abe**

Abstract (167Words)

The synthesis of pure brookite is generally much more difficult than that of pure anatase. The hydrothermal conversion, recently developed by Kozawa et al., is a facile method to synthesize brookite TiO_2 from inverse spinel-type Mg_2TiO_4 under a mild hydrothermal condition e.g. in 1 M HCl solution at 100 °C. However, slight rutile TiO_2 is usually co-existed under the reported conditions. The aim of this study is to prepare a high-purity brookite TiO_2 powder by the hydrothermal conversion from Mg_2TiO_4. We investigated the conditions of Mg_2TiO_4 preparation and hydrothermal conversion, and it was found that the most important factor for the high-purity brookite synthesis, i.e. decreasing the co-existing rutile TiO_2, was to prepare the Mg_2TiO_4 precursor without $MgTiO_3$. Using an MgO-rich composition and adding a second calcination step for the Mg_2TiO_4 preparation yielded a high-purity (99.3 wt%) brookite powder with a surface area of 27.7 m^2/g. Under the current experimental conditions, addition of a surfactant or an alcohol for the hydrothermal treatment was not apparently effective for the high-purity brookite synthesis.

Keywords

Chemical preparation; -TiO_2; Spinels; Mg_2TiO_4

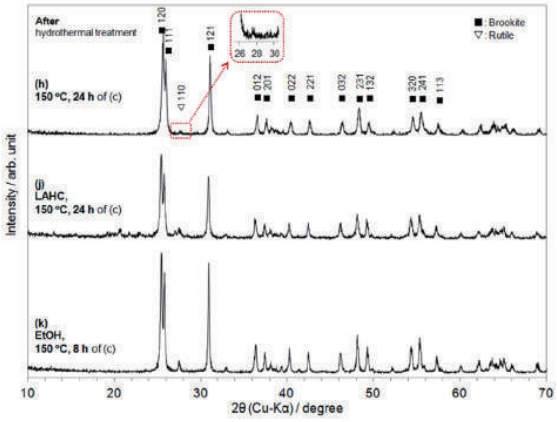

Fig.1 XRD patterns of the samples after the hydrothermal treatment using sample (c): (h) at 150 °C for 24 h, (j) at 150 °C for 24 h with LAHC, and (k) at 150 °C for 8 h with EtOH.

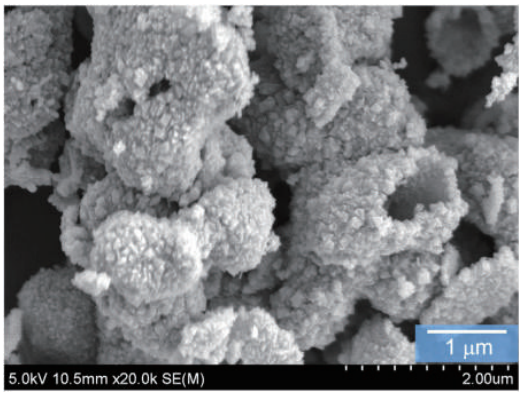

Fig.2 SEM micrograph of the brookite powder, sample (h), with the surface area of 27.7m^2/g.

* University of Tsukuba
** Associate Professor

71st IIW Annual Assembly and International Conference, Bali, Indonesia, (2018.07.15-2018.07.20), Doc. 212-1560-18

Fundamental Study on Welding Phenomena of Submerged Arc Welding with X-ray Observation

Yohei ABE*, Takahiro FUJIMOTO**, Mitsuyoshi NAKATANI ***, Hisaya KOMEN****, Masaya SHIGETA*****, Manabu TANAKA******

Abstract (126 Words)

Submerged arc welding (SAW) is a consumable electrode type arc welding widely used for butt welding of thick plates in industrial equipment because of its high deposition rate and high weld quality. Recently, higher efficiency and automatic welding are available due to accurate digital waveform control and improved reproducibility. The SAW is a complicated welding process involving multiple welding phenomena, arc, droplet transfer, flux evaporation, slag solidification, and more, these are few investigation because the phenomena are blanketed by flux. In this study, X-ray observation is used to evaluate the SAW welding phenomena. We performed 3,000 frames/s of high-speed X-ray observation, and investigated droplet transfer, as well as solidification of slag during SAW. In addition, we discussed the influence of welding speed on the welding phenomena.

Keywords

Submerged arc welding; Welding phenomena; X-ray observation

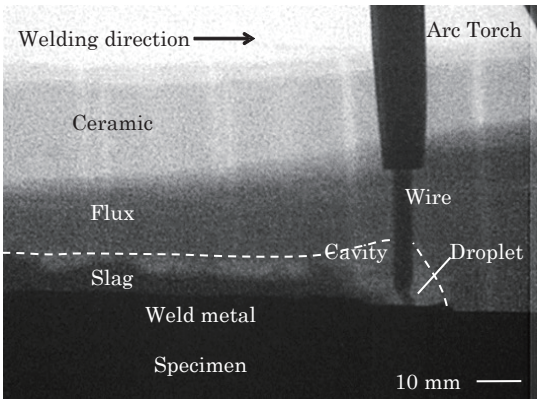

Fig.1 High-speed observation result with X-ray

	Welding speed		
	30 cm/min	35 cm/min	43 cm/min
Cross section of weld bead	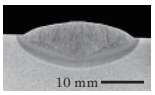	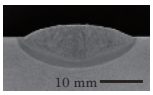	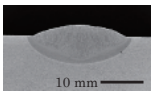
Cross section of slag			

Fig. 2 Cross sections of weld bead and slag at various welding speeds

* Specially Appointed Assistant Professor
** Hitachi Zosen Corporation
*** Specially Appointed Associate Professor
**** Graduate School Student
***** Associate Professor
****** Professor

Optics and Lasers in Engineering, 101, (2018), 23-27.
doi:10.1016/j.optlaseng

The effect of particle size on the heat affected zone during laser cladding of Ni–Cr–Si–B alloy on C45 carbon steel

-

Daichi Tanigawa*, Nobuyuki Abe**, Masahiro Tsukamoto*****, Yoshihiko Hayashi****, Hiroyuki Yamazaki***, Yoshihiro Tatsumi******, Mikio Yoneyama******

Abstract (154 Words)

Laser cladding is one of the most useful surface coating methods for improving the wear and corrosion resistance of material surfaces. Although the heat input associated with laser cladding is small, a heat affected zone (HAZ) is still generated within the substrate because this is a thermal process. In order to reduce the area of the HAZ, the heat input must therefore be reduced. In the present study, we examined the effects of the powdered raw material particle size on the heat input and the extent of the HAZ during powder bed laser cladding. Ni–Cr–Si–B alloy layers were produced on C45 carbon steel substrates in conjunction with alloy powders having average particle sizes of 30, 40 and 55 μm, while measuring the HAZ area by optical microscopy. The heat input required for layer formation was found to decrease as smaller particles were used, such that the HAZ area was also reduced.

Keywords

Composite materials; Microporous materials; Electrical characterization; Rietveld analysis

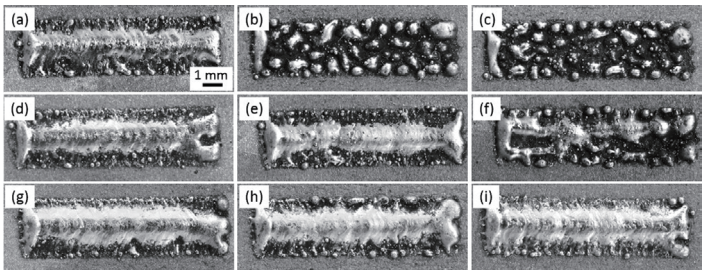

Fig. 1. Optical microscope images of cladding layer surfaces for heat inputs of (a–c) 162.5, (d–f) 200 and (g–i) 250 Jcm^{-1}, and alloy particle sizes of (a, d and g)

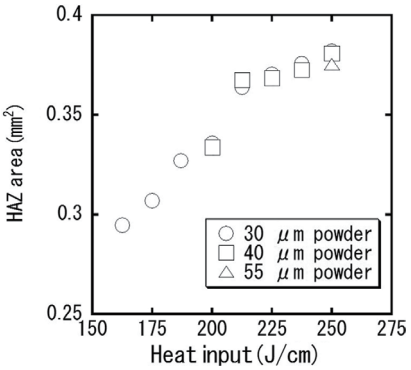

Fig. 2. HAZ areas as functions of heat input when using (○) 30, (□) 40 and (Δ) 55 μm alloy particles.

* Graduate School Student
** Specially Appointed Professor
*** Professor
**** Specially Appointed Assistant Professor
***** Specially Appointed Associate Professor
****** Guest Researcher

The 3rd International Symposium on Creation of Life Innovation Materials for Interdisciplinary and International Researcher Development (iLIM-3), Program and Abstract Book (2018) P-15

Synthesis of Tailor-Made Ceramic Nanocrystals by Organic Ligand-Assisted Hydrothermal Method towards Environmental Applications

Satoshi Ohara*

Abstract (102Words)

To fine-tune the properties of ceramics, they can now be processed into uniform-size nanocrystals with spherical, wire, rod, tadpole shapes. Another trend in research aims at arranging individual nanocrystals into superlattices and investigating their unique properties. Despite these recent advances, controlling the shape, crystal structure, and surface characteristics of ceramic nanocrystals is still a difficult task. We report an approach to tailor-made ceramic nanocrystals by means of organic ligand-assisted hydrothermal method towards environmental applications. We succeeded in the synthesis of the ceramic nanocrystals such as ceria (CeO_2) nanocubes, as shown in Figure 1, and titania (TiO_2) nanosheets, as shown in Figure 2.

Keywords

Hydrothermal; Nanocrystals; CeO_2; Gd-doped CeO_2; TiO_2

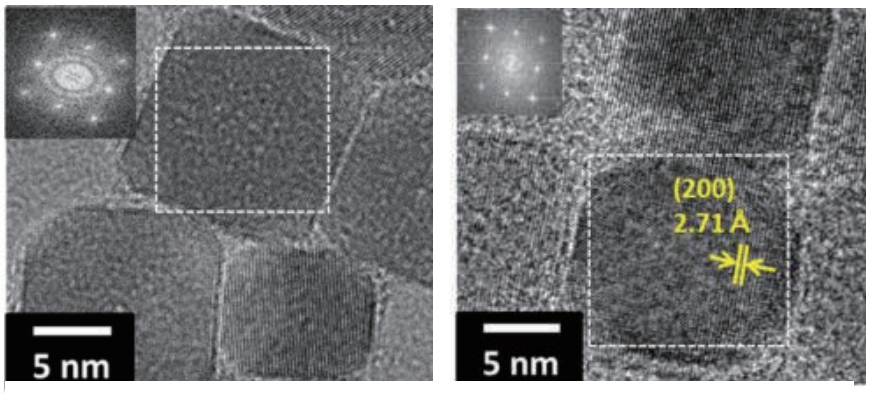

Fig. 1. CeO_2 (left) and Gd-doped CeO_2 (right) nanocubes.

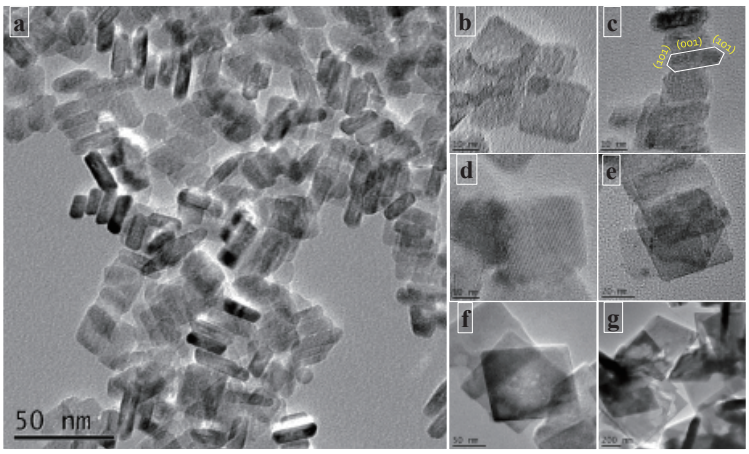

Fig. 2. TiO_2 nanosheets.

* Specially Appointed Professor

Activity report on "The Project to Create Research and Educational Hubs for Innovative Manufacturing in Asia"

Katsuyoshi KONDOH*, Hiroshi NISHIKAWA*, Mihoko KATSUMATA**,
Chie HASHIMOTO ***, Misa TERANISHI****

Abstract (242 Words)

The project has started the Phase II from this year. In Phase II, two main objectives were set; 1) Strongly commit with the international collaboration researches to publish the co-authored papers by continuously enhancing the plat form of research network in Greater Asia Region, 2) Implement oversea internships which tie up students from different area of science and the humanities, named as Coupling Internship (CIS). Results of this year's activities were reported as below.

1) Total of 23 international collaboration researches including 18 newly commenced and 5 continuous researches from Phase I were implemented. 3 workshops with National Taiwan University, Vietnam Academy of Science and Technology, and Hanoi University of Science and Technology were respectively organized. Through the collaboration researches shown in Table 1, about 34 international co-authored papers are expected to be submitted during this year.
2) Coupling Internship was conducted in 7 locations. 5 out of 7 were called Out-bound CIS conducted in Thailand, Vietnam, Myanmar, Indonesia, and in India whereas other 2 were called In-bound CIS conducted inside Japan at Aioi city and at Rokko city in Hyogo. In-bound CIS was newly started from Phase II. Pictures from CIS can be found in Fig. 1 and Fig. 2.
3) Based on the international collaboration research networks, JWRI received 10 students from the partner universities in Taiwan, Thailand, India, and China who conducted researched by using internship scheme as well as by using JST Sakura Science Plan scheme (short program).

Table 1 – List of International Joint Research in 2018 (abstract)

Partner University	Research Topics
Shang Hai Jiao Tong University (China), Korea University (Korea)	Evaluation method of toughness of dissimilar joint at Charpy impact test
Nanyang Technological University (Singapore)	High strengthening mechanism of light metals fabricated by 3D printing (SLM) process
National Cheng Kung University (R.O.C), King Saud University (Saudi Arabia)	Low temperature bonding required for packaging of organic devices such as wearable devices
Beijing University of Technology (China)	Elucidation of melt pool formation process in AC plasma welding of aluminum alloy
Chulalongkorn University (Thailand)	Solid-solution of Zr atom in Ti sintered materials and their strengthening mechanism
Indian Institute of Technology Hyderabad (India)	Elucidation of melting phenomenon of waveform control SAW
King Mongkut's University of Technology, Thonburi (Thailand), Northwestern Polytechnical University (China), Chinese Academy of Science (China)	Thermal decomposition mechanism of oxides and nitrides in Ti sintered materials and evaluation of their microstructural and mechanical properties

Fig. 1 CIS Daihen (Rokko, Japan)

Fig. 2 CIS ISGEC/Hitachi Zosen (India)

* Professor
** Specially Appointed Associate Professor
*** Specially Appointed Lecturer
**** Specially Appointed Assistant Professor

J. of Smart Processing for Materials, Environmental & Energy, 7, 2 (2018), 65–72
スマートプロセス学会誌，ISSN 2186–702X

Study of improvement of power and stability of magnesium air battery – influence of cathode materials and structure on battery properties –

マグネシウム空気電池の高出力・安定化に関する研究―正極材料・構造の電池特性への影響－

Keijirou ITAKURA*, Takahiro TSUTSUI**, Zhonghao HENG***, Hirohisa HIRAKI****, Shigeaki UCHIDA*, Yasuo TAKAHASHI*****

板倉 啓二郎*，筒井 剛大**，衡 中皓***，平木 博久****，内田 成明*，高橋 康夫*****

Abstract (127 Words)

Power and energy dependences of magnesium air batteries on the materials and structures of carbon cathodes are investigated for the purpose of developing a high-power Mg-air battery. It is found that three-phase co-existing interface plays an important role to improve the power and energy properties. A new cathode structure having an enhanced cathode reaction was developed. The Mg-air battery with this new cathode generated 5 times more power and 2.5 times more energy, compared to that of conventional cathodes. Moreover, the cathode with a three-layered structure was fabricated for obtaining a better current density. The high-power battery cell showed 72W/kg of power density and 400Wh/kg of energy density, which revealed a potential ability for various application, such as mobile phone, electric vehicle, and high-power emergency power supply.

Keywords

Magnesium; Air battery; Carbon cathode; Oxygen reduction reaction; Fuel cell; Flooding; Interfacial chemical reaction

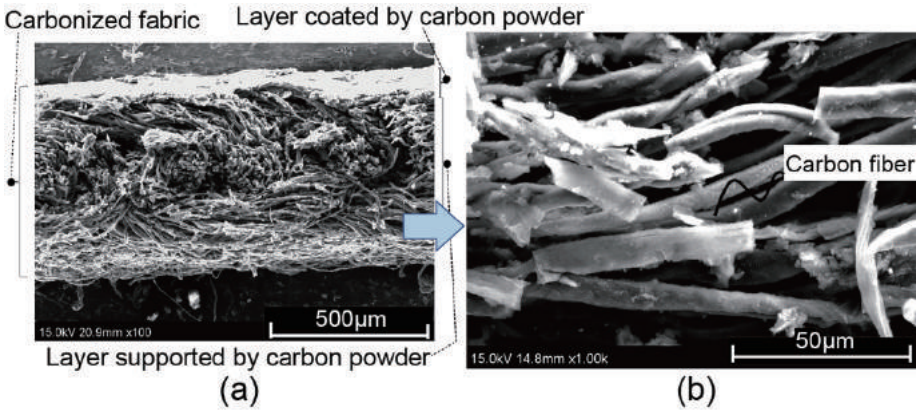

Fig. 1 SEM photos of cross-sectional surfaces of the cathode of Mg air battery.
(a) x100 and (b) Enlarged photo.

* Guest Professor
** Graduate School Student
*** Specially Appointed Researcher
**** Guest Associate Professor
***** Specially Appointed Professor

Journal of the European Ceramic Society, 37, (2017), 5339-5345.
doi:10.1016/j.jeurceramsoc.2017.05.056

Spherical porous granules in MgO-Fe_2O_3-Nb_2O_5 system: *In situ* observation of formation behavior using high-temperature confocal laser-scanning microscopy

Yoshikazu Suzuki*, Hiroya Abe****, Hajime Yamamoto***, Kazuhiro Ito*****, Hiroshige Inoue*****, Mayumi Nakamura**

Abstract (109Words)

The pyrolytic reactive granulation process, yielding ceramic spherical porous granules, is simple, consisting of typical ceramic processing methods, viz., wet-ball milling of powders, vacuum drying, granulation via sieving through a screen mesh, and one-step heat treatment for local reactive sintering within each granule. Here, the microstructural development of spherical porous granules was successfully visualized by in situ high-temperature confocal laser-scanning microscopy during the heating up to 1400 °C in air. Based on the result of the in situ observation, a simple but powerful size-controlling process of spherical porous granules, viz., multiscreen sieving after the heating was demonstrated. Nearly monodispersed spherical porous granules composed of pseudobrookite-type $MgFeNbO_5$ were easily obtained.

Keywords

Spherical porous granule (SPG); *In situ* observation; Confocal laser-scanning microscopy (CLSM); Pseudobrookite; $MgFeNbO_5$

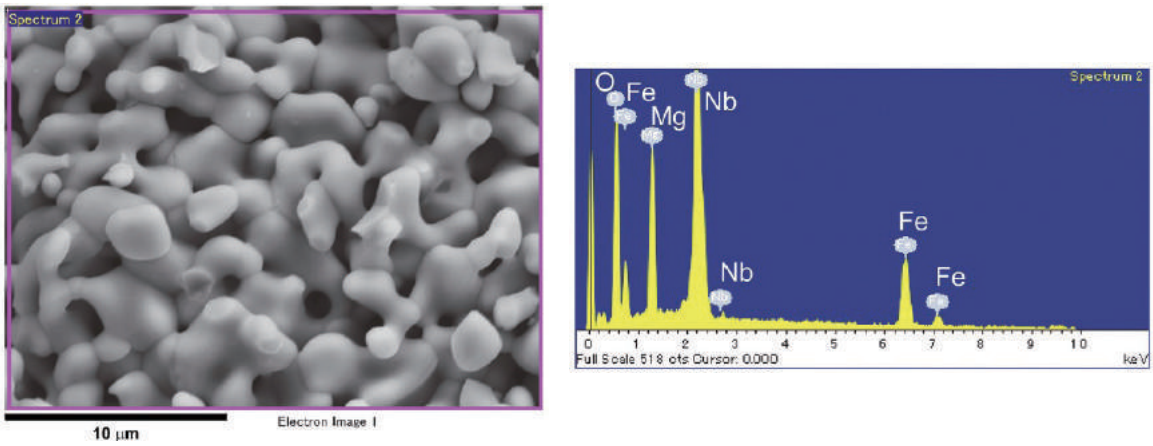

Fig.1.
SEM-EDS wide-area analysis of a $MgFeNbO_5$ SPG, showing 11.6 at.% Mg, 11.9 at.% Fe, 12.1 at.% Nb and 64.5 at.% O, which are close to the ideal composition of $MgFeNbO_5$:12.5 at% of each metal and 62.5 at% of oxygen.

* University of Tsukuba
** Yonekura MFG Co.
*** Graduate School Student
**** Associate Professor
***** Professor

Proceedings of the 6th International Conference on Crack Paths (CP 2018), (2018), 395–400.

Control Factor of the Roughness of the Cleavage Fracture Surface in Polycrystalline Steel

Tomoya Kawabata*, Fumiaki Tonsho**, Yuki Nishizono***, Yasuhito Takashima ****

Abstract (192Words)

Brittle fracture in carbon steel affects serious impact for the safety of fracture of in steel structure. Thus, the arresting technology of crack propagation is the last stand for the structure. It is so important issue that the conditions which can be stopped reliably crack propagation should be clarified thoroughly. On the background of such social importance, lots of experimental and theoretical researches have been conducted from both mechanical and microstructural viewpoints. Fracture surface roughness is an important factor in studying the physics of dynamic high speed crack propagation. For example, in the resin material, the fracture surface roughness is increased corresponding to the crack propagation speed called Mirror-Mist-Huckle, and it is known that when crack propagation speed is further accelerated, cracks macroscopically branch off. However, the authors have already revealed that the critical conditions of branching in steel, but have already found that crack branching occurs under conditions of high stress triaxiality, not in high speed conditions as seen in resin materials. In this study, in order to elucidate the controlling factor of the process of increasing the fracture surface roughness and branching, experimental investigation using numerical analysis was carried out.

Keywords

Steel; Brittle crack propagation; roughness; dissipation energy

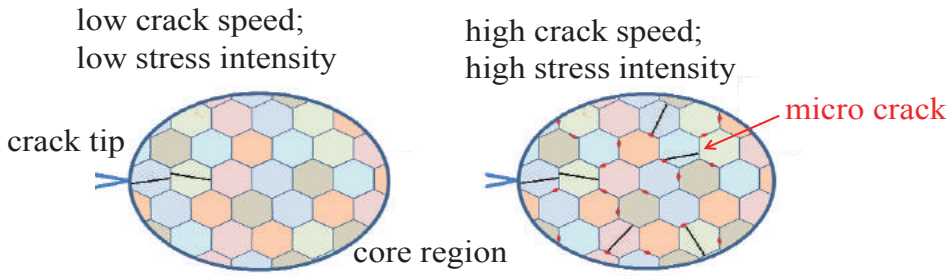

Fig. 1.
Schematic explanation of microscopic mechanism of increase of fracture surface roughness under high stress and stress triaxiality condition.

* University of Tokyo
** University of Tokyo
*** University of Tokyo
**** Assistant Professor

Multi-Dimensional Additive Manufacturing (2018) 35-46, Soshu Kirihara* and
Kazuhiro Nakata** Eds., The Japan Welding Engineering Society, ISBN: 978-4-907200-08-4

Principles of Electron Beam Melting

Yuichiro Koizumi***, Akihiko Chiba ***

Abstract (136 Words)

Electron beam melting (EBM) is an additive manufacturing technique that is characterized by irradiating powder of raw metal materials using an electron beam. Two-dimensional (2D) slice data are acquired from three-dimensional (3D) geometrical data of the target object, the process of manufacturing based on 2D slice geometries is repeated many times, and the 3D target object is obtained by laminating them. This procedure is in common with many other additive manufacturing methods. The basic difference from laser additive manufacturing is simply whether the heat source is an electric beam or laser, but pertaining to this difference, various differences exist including the atmosphere of manufacturing process, temperature, and size of used powder. In this chapter, the principle of EBM is explained with particular consideration to the difference from laser melting, and characteristics unique to EBM are emphasized.

Keywords

Electron beam melting; Additive Manufacturing; Metal Powder

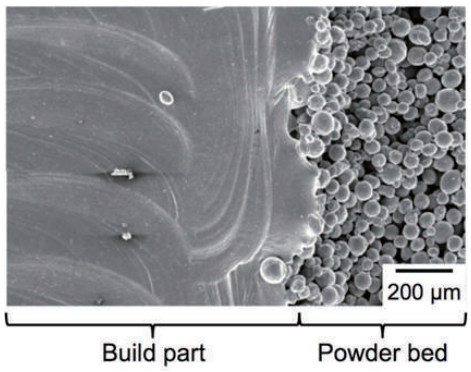

Fig. 1 An interface between build part (left) and powder bed (right).

Fig. 2 EBM-built artificial knee joints after polishing.

* Professor
** Emeritus Professor
*** Tohoku University